Available online at www.sciencedirect.com
SCIENCE DIRECT
ELSEVIER
Journal of the European Ceramic Society 26 (2006) 949–956
ECERS
www.elsevier.com/locate/jeurceramsoc

Dip-coating technique for the manufacture of alumina microfilters using PVA and Na-CMC as binders: a comparative study

Cavus Falamaki*, Mahdi Naimi, Alireza Aghaie

Ceramics Department, Materials and Energy Research Center, P.O. Box 14155-4777, Tehran, Iran

Received 25 May 2004; received in revised form 6 November 2004; accepted 26 November 2004
Available online 19 January 2005

Abstract

α-Alumina microfiltration flat-membranes have been prepared using the dip-coating procedure. The effect of slip concentration (<30 wt.%), coating time and binder type (PVA and Na-CMC) on the thickness, porosity, roughness and effective pore diameter of the membrane layers has been investigated. A new method for the characterization of the membrane layer based on gas permeation has been presented and the pertaining equations derived. The method is applicable if permeability measurements embrace both Knudsen and Poiseuille flow regimes.

Keywords: Membranes; Al_2O_3; Binders; Filters; Slip casting

1. Introduction

Despite the available vast open literature concerning the dip-coating and sintering of "nanopore" layers on ceramic supports, much less has been disclosed regarding the same process for layers known as microfilters. Recall that in the liquid–solid separation domain, ceramic microfilters have already found widespread industrial application while ceramic nano and ultrafilters are still mainly a subject of academic research.

In the manufacture of composite membranes through dip-coating, the control of the deposited layer thickness is crucial. The minimum layer thickness is of the order of the maximum in substrate surface roughness.[1] In practice, layer thicknesses for microfilters are in the range of 20–30 μm.[2] Gu and Meng[3] studied the influence of the dipping time on the thickness of α-alumina microfilters prepared by dip-coating. The membrane characteristics (such as the effective pore diameter) and the effect of other controlling parameters were not considered. It is the aim of the present work to study the effect of slip concentration, coating time and binder type on the thickness, porosity, roughness and effective pore diameter of α-alumina microfilter layers prepared by the dip-coating method. It is shown that the linear relationship between the thickness of the sintered membrane and the square root of time proposed by Gu and Meng[3] is generally invalid.

In addition, a new method for the characterization of the sintered membrane layer based on gas permeation has been disclosed and the pertaining equations have been derived. The method is applicable if permeability measurements embrace both Knudsen and Poiseuille flow regimes.

2. Experimental

The α-alumina substrates were prepared according to the optimum procedure reported elsewhere.[4] These had an average open porosity of 0.41 and a surface roughness (R_a) in the range of 0.6–0.8 μm.

The substrates were coated using a dip-coating technique. A Martoxide alumina powder (ZS-402/M) with a specific surface area of 7 $m^2\ g^{-1}$ was used for the preparation of aqueous slips. PVA (4 cm^3 per 100 g solid, 2 wt.% aqueous solution)

* Corresponding author. Fax: +98 0262 62 21 888.
E-mail address: cavus_falamaki@yahoo.com (C. Falamaki).

0955-2219/$ – see front matter © 2004 Elsevier Ltd. All rights reserved.
doi:10.1016/j.jeurceramsoc.2004.11.018

was used as binder in one series of the experiments to prevent cracking during drying. For this set of experiments STPP (2 g per 1000 g solid) was used as dispersing agent. In another set of experiments, sodium carboxymethylcellulose (Na-CMC) was used as binder. No additional dispersing agent was added as the latter slip was relatively stable in the alumina concentration range under study. The slip was planetary milled for 30 min to break any agglomerates formed. In the case of slip viscosity and particle size distribution determination, the measurements were performed immediately after the fast milling step. The dipping was also performed immediately after the fast milling step. The coating was done manually in an open beaker on one side of the support disks. The withdrawal speed was approximately $0.02\,m\,s^{-1}$. This was accomplished by covering the other side using an adhesive-tape. The samples were initially dried at room temperature for 24 h and then at 60 °C overnight. Afterwards, the samples were heated up to the sintering temperature (1150 °C)with a heating rate of $3\,^{\circ}C\,min^{-1}$. The soaking time was 1 h.

Dry and wet N_2 permeability tests were performed according to ASTM F316 using a special holder made in our laboratory.[5] Wet permeability tests were done using paraffin as saturation medium. Particle size distribution measurements were done using the light scattering technique (Fritsch, Analysette 22). Surface roughness was measured using a TR 100 surface roughness tester (TIME). Micrographs were taken using a Stereo Scan 360-Leica (Cambridge) instrument. Viscosity measurements were performed using a Brookfield RTV DV-III rotating-spindle viscometer. In some cases, the thickness of the coatings had been determined by observing carefully polished sections of the samples with a light microscope (Metallux, Leitz).

3. Results and discussion

3.1. Slips containing Na-CMC

Preliminary experiments showed that, in the concentration range of 10–30 wt.% alumina, Na-CMC acted as a binder and effective deflocculant simultaneously. Addition of a dispersing agent like STPP increased flocculation and eliminated slip stability.

A series of experiments concerning slip rheology was performed from which the results are necessary for the next discussion. The slip viscosity is a determining factor of membrane thickness and the compactness of the precursor particles.[6] Apparent viscosity as a function of slip concentration and shear rate has been shown in Fig. 1. The term apparent alludes to the low magnitudes of torque during the experiments which makes the observed viscosity data prone to some error but usable for comparison means. It is observed that viscosity increases with increasing shear rate showing that the slip behaves as a dilatant fluid.

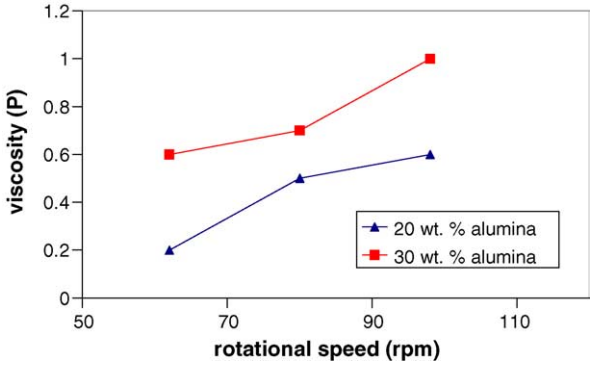

Fig. 1. Viscosity as a function of rotational speed for the slips containing Na-CMC as binder.

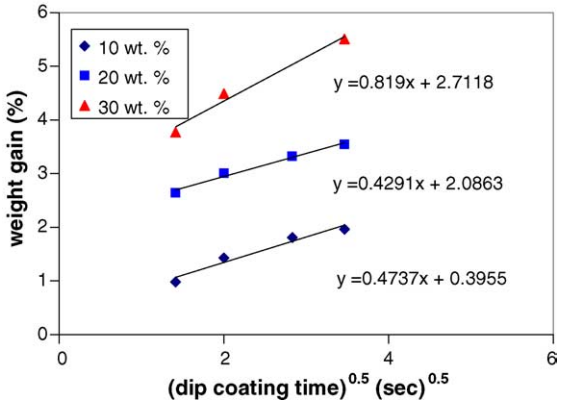

Fig. 2. Weight gain as a function of dip-coating time and slip concentration of the sintered samples (Na-CMC used as binder).

A simplified equation for the evaluation of the layer thickness during the dip coating process is as follows[7]:

$$L = \left[\frac{2P}{\mu[((\varepsilon/\phi)-1)[(1/K_{avg})+((\varepsilon/\phi)-1)/\varepsilon_s K_s]]}\right]^{0.5} t^{0.5} \quad (1)$$

where L is the membrane layer thickness (m); t, time (s); P, the total filtration pressure (Pa) which is equal to the average capillary suction pressure caused by the substrate; μ, the slip viscosity ($kg\,m^{-1}\,s^{-1}$); ε, the average membrane void volume fraction; ϕ, the slip volume fraction of solids; K_{avg}, the average permeability of the consolidated layer (m^2); ε_s, the substrate porosity; and K_s, the substrate permeability (m^2).

Fig. 2 shows the weight gain of the sintered samples as a function of dip-coating time and slip concentration. A linear relationship between weight gain and the square root of time exists. If the variation of coat porosity with dip-coating time is neglected (negligible particle aggregation, incompressible cake), the thickness is directly proportional to the weight gain, and therefore, Eq. (1) holds. Then, referring to the same figure, it might be concluded that increasing slip concentration from 10 to 20 wt.%, the slope decreases slightly mainly because of viscosity increase. Increasing the slip concentration

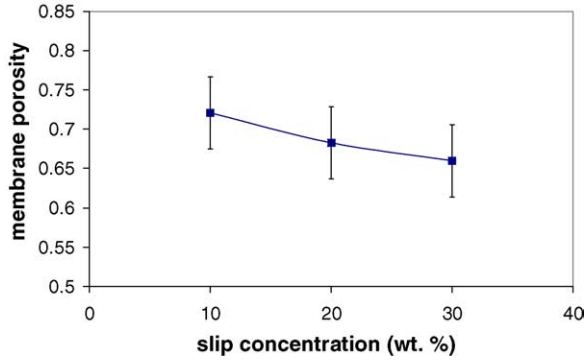

Fig. 3. Average porosity of the sintered layers as a function of slip concentration (Na-CMC used as binder).

up to 30 wt.% results in a higher slope due to the dominant effect of a higher value of ϕ.

Referring again to Fig. 2, the existence of an additional "adhering layer" on the slip-coated film is observed for all the slip concentrations under consideration. Extrapolation of each line to the point corresponding to zero time gives us the weight of the adhering layer. The latter increases as the slip concentration increases. This is mainly attributed to a higher slip solid content, as during the experiments, the volume of the adhering liquid seemed to be approximately constant for each case.

Fig. 3 shows the average porosity of the sintered membrane layers as a function of slip concentration. The latter has been calculated using the weight gain (W), layer thickness (t) and membrane surface area (A) through the following relation:

$$1 - \varepsilon = \frac{W}{\rho A t} \tag{2}$$

where ρ is the density of α-alumina. Porosities are in the range of 0.65–0.72 and follow a decreasing trend with respect to slip concentration increase. Fig. 4 shows an SEM picture

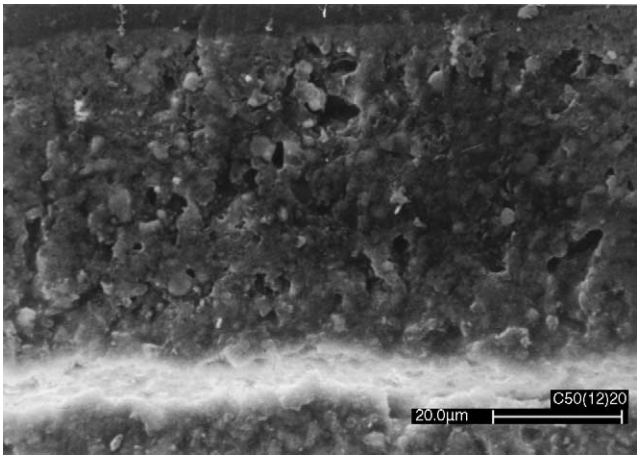

Fig. 4. SEM picture of the cross section of a sintered sample (Na-CMC used as binder). Slip concentration and dip-coating time had been 20 wt.% and 12 s, respectively.

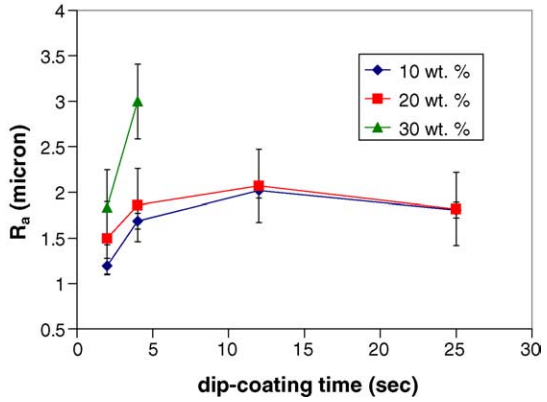

Fig. 5. Variation of surface roughness (R_a) as a function of dip-coating time and slip concentration (Na-CMC used as binder).

of a sample using a 20 wt.% alumina slip concentration and a dip-coating time of 12 s. Significant inhomogeneity in micropore structure across the cross section is observed. We observed such an inhomogeneity in all the samples for which Na-CMC was used as binder. Fig. 5 shows the variation of the sample roughness (R_a) as a function of slip concentration and slip coating time. It is observed that roughness increases with increasing slip concentration for a specified dip-coating time. Surface roughness is interrelated with the aforesaid sample inhomogeneity. There exists an abrupt increase in R_a from a 20 to 30 wt.% slip concentration. This might be attributed to the higher casting rate (approximately double) in the case of 30 with respect to 20 wt.% slip concentration. Considering slip concentrations 20 and 10 wt.% alumina, R_a initially increases sharply and afterwards decreases slightly. The rising section also exists for the 30 wt.% slip concentration. These results point towards the fact that during the coating process, particles approaching the substrate tend to agglomerate as more time is elapsed.

Fig. 6 shows the sintered layer thickness as a function of the square root of time and slip concentration. If it is attempted to fit a straight line to the data points corresponding to each slip concentration, it emerges that the correlation factor becomes significantly poorer as slip concentration increases.

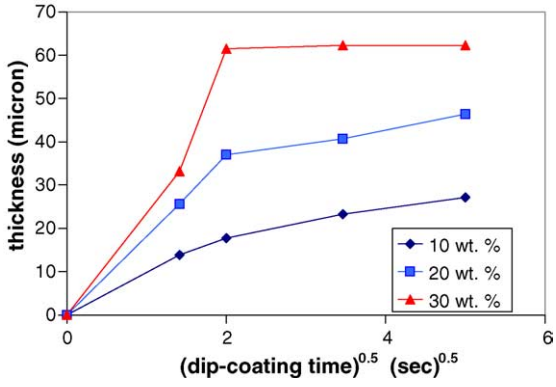

Fig. 6. Sintered layer thickness as a function of square root of time and slip concentration (Na-CMC used as binder).

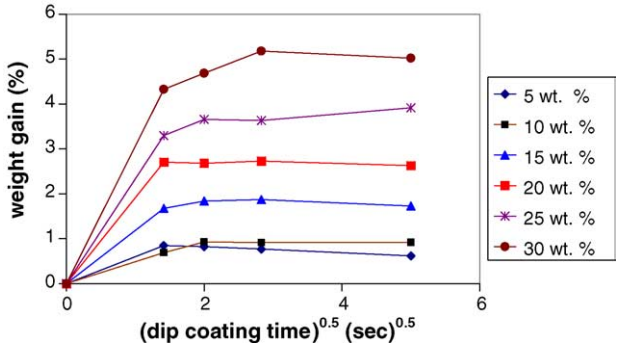

Fig. 7. Weight gain as a function of dip-coating time and slip concentration of the sintered samples (PVA used as binder).

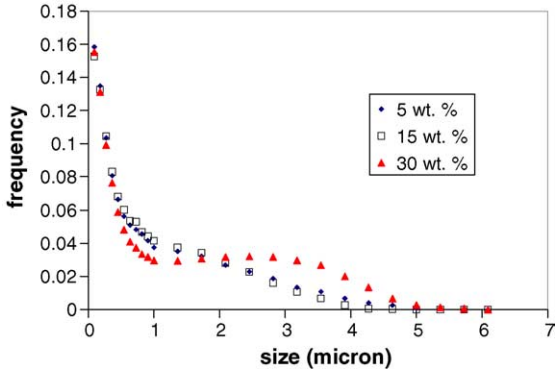

Fig. 8. Particle size distribution within the slip as a function of slip concentration (PVA used as binder).

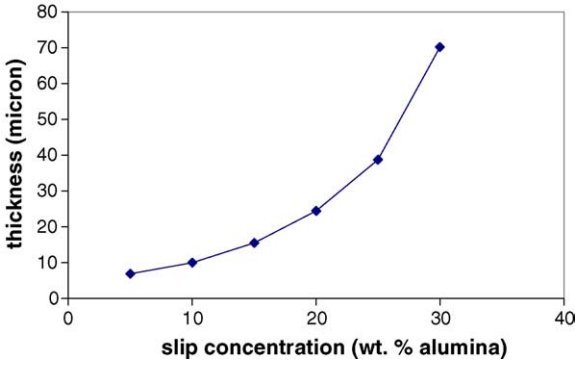

Fig. 9. Sintered layer thickness as a function of slip concentration for a dip-coating time of 25 s (PVA used as binder).

Gu and Meng[3] derived a linear relationship between the thickness of the sintered membrane and the square root of time. They assumed a constant porosity for the sintered membrane layers prepared at different coating times at constant slip concentration. Our results clearly show that such a relationship is here invalid. The experimental data presented in the previous paragraph support the fact that for a constant slip concentration, the state of agglomeration in a direction normal to the membrane surface is subject to variation. On the other hand, the initial particle packing characteristics (porosity and pore size distribution) are well-known to have a determining effect on the process of solid-state sintering (final shrinkage and porosity).[8] Hence, even if the wet membrane porosity remains approximately constant with dip-coating time, different shrinkages will result in different final porosities.

3.2. Slips containing PVA and STPP

Fig. 7 shows the weight gain of the sintered samples as a function of dip-coating time and slip concentration. It is observed that for a slip concentration range of 5–25 wt.%, the coating process is relatively fast and maximum weight gain takes place in less than 2 s.

It had not been possible to perform the dip-coating process in periods less than 2 s because of experimental difficulties like high submerging speeds resulting in suspension turbulence and inaccuracy of time measurements.

Fig. 8 shows the effect of slip concentration on the particle size distribution after the planetary milling step. Large agglomerates up to 130 μm are observed to exist for slip concentrations 5, 15 and 30 wt.% alumina. Nevertheless, their fractional volume is negligible. On the other hand, except for the 30 wt.% concentration, the general trend of the curves is almost the same. Table 1 summarizes the geometric mean diameter of the slips. A slight increase with increasing slip concentration is observed which may be reasonably attributed to more agglomeration because of higher concentrations used.

Fig. 9 shows the effect of slip concentration on the thickness of the sintered samples for a constant dip-coating time of 25 s. A nonlinear relationship is observed. Actually, if the porosity (Φ_m) of the membrane coatings prior to sintering were approximately the same, according to the approximate direct proportionality between weight gain and slip concentration(Fig. 7), we would have expected a similar shrinkage behavior during sintering. In other words, the experimental points in Fig. 9 should be more or less on a straight line. Taking into account the observation that the slip particle size distribution is a weak function of slip concentration within the range under study, the trend observed in Fig. 9 may be attributed to a difference in initial porosity. Recall that higher porosities accompanied with inherent large packing inhomogeneities may lead to significant less consolidation. Fig. 10 shows the average porosity of sintered membrane layers as a function of slip concentration. It is observed that porosity increases with increase of slip concentration. As the relative amounts of binder and stabilizer per gram dry powder have been taken constant for each slip concentration, the degree of compaction should not be a significant function of slip concentration due to the repulsive–attractive

Table 1
Geometric mean diameter as a function of slip concentration for the slip containing PVA and STPP

Slip concentration (wt.% alumina)	Geometric mean diameter (μm)
5	0.40
15	0.42
30	0.45

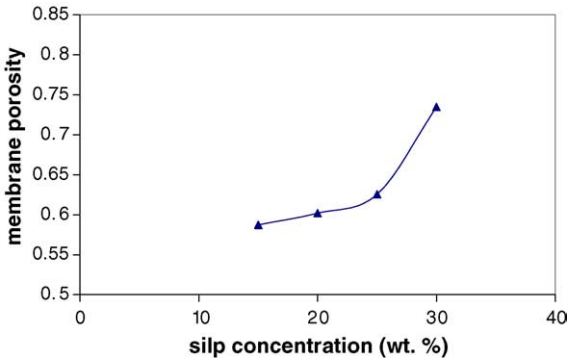

Fig. 10. Average porosity of the sintered layers as a function of slip concentration (PVA used as binder).

forces between particles. Fig. 11 shows the bubble point test results for the sintered samples using different initial slip concentrations. The latter test gives an approximate evaluation of the maximum effective pore size within the membrane layer. It is clearly observed that increasing slip concentrations result in larger pores. Fig. 12 shows micrographs of coatings obtained for 15 and 25 wt.% slip concentrations. It is presumed that the casting rates increase with slip concentration in the range under study. This is possible as, referring to Eq. (1), increasing slip solid content increases the coating rate if the effect of viscosity increase is not significant. Therefore, it may be presumed that higher porosities with increasing slip concentrations are mainly due to a more violent mass transfer of particles resulting in less compact layers.

Fig. 13 shows how pinhole defects due to entrapped air may develop during the dip-coating process. The bubbles have an appreciable size (almost of the same order of the layer thickness), and therefore, may be detrimental. Such defects could be observed for slip concentrations equal and larger than 30 wt.% alumina. It should be mentioned that for gas permeation modeling, the sample corresponding to the 30 wt.% slip concentration was deprived of such defects, according to optical and scanning electron microscopy inspections. Slip de-airing is an essential step in processing slips in the latter

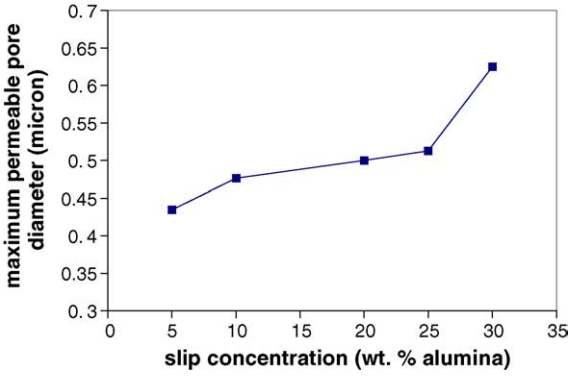

Fig. 11. Maximum permeable pore diameter as a function of slip concentration for a coating time of 25 s (PVA used as binder).

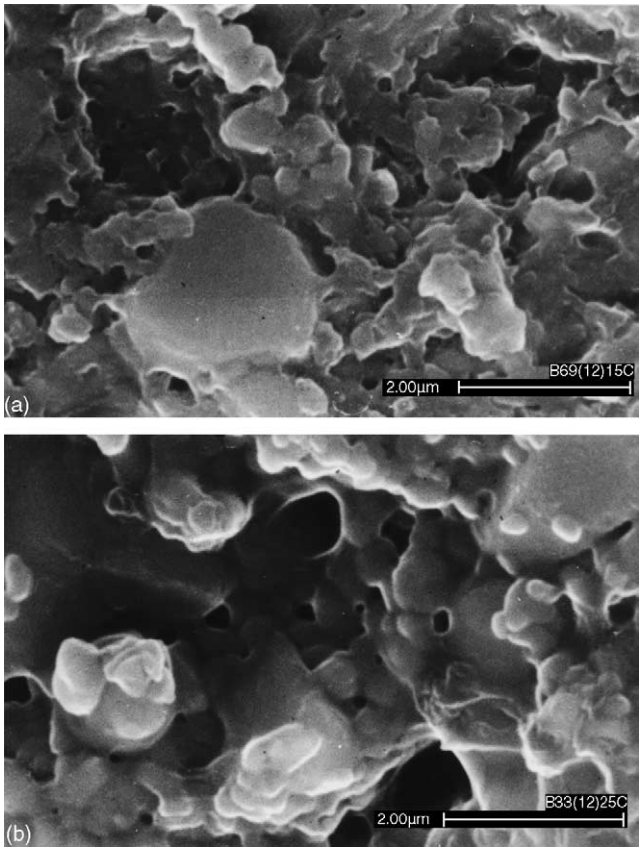

Fig. 12. SEM pictures of cross sections of sintered coatings using PVA as binder: and a dip-coating time of 12 s: (a) 15 wt.% and (b) 25 wt.% slip concentration.

concentration range. This may be achieved by addition of a surfactant and conditioning for some period of time.[9]

The results of surface roughness R_a measurements were rather scattered averaging about 1.85 μm. However, the standard deviation followed an increasing trend with slip concentration increase and decreasing trend with the time of dip-coating (Fig. 14).

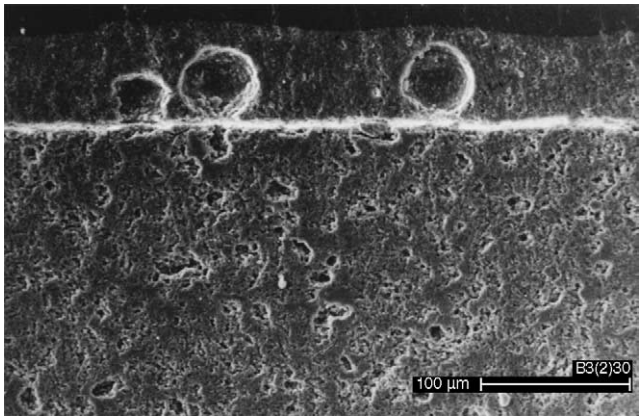

Fig. 13. Pinhole defects at the slip–substrate interface of a sintered sample for a slip concentration of 30 wt.% and a coating time of 2 s (PVA used as binder).

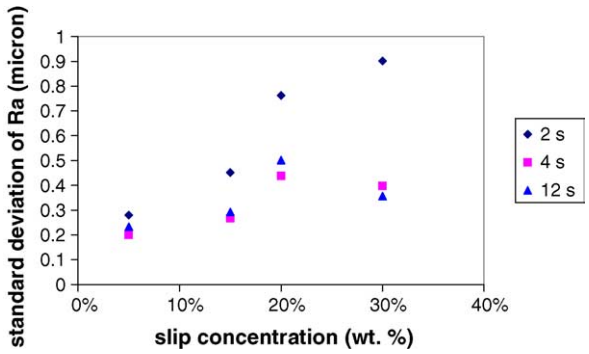

Fig. 14. Standard deviation of R_a for the samples prepared using PVA as binder.

At this stage, it is useful to discuss the efficiency of the dip-coating comparing actual and maximal weight gain.. Considering the open void volume of the substrate, it is possible to evaluate the theoretical amount of the saturation weight gain. The latter is calculated as the product $V_s \times \varepsilon_s \times C_{slip}$ where V_s is the substrate volume; ε_s, the substrate porosity; and C_{slip}, the slip concentration. Referring to Fig. 15, it is observed that the saturation weight gains are much less. The latter is in the range of 13–18% for PVA and 20–28% for Na-CMC. One possible cause might be a different hydrodynamic state near the cake-slip interface which is responsible for the retrogression of some of the solid particles to the bulk of the slip slurry. More retrogression is observed in the case of PVA used as binder. On the other hand, a large part of the coating can "disappear" as the substrate is drawn out of the suspension due to the instability of the "mobile" part of the formed membrane layer cake.

3.3. Modeling of gas permeation

In order to evaluate the structural parameters of the membrane layers, gas permeation has been modeled based on the methodology presented by Falamaki et al.[10] The highlight of the latter work is that the permeability of a membrane support (without coating) is measured over a wide range of pressure drops. Accordingly, the flow regimes belonging to

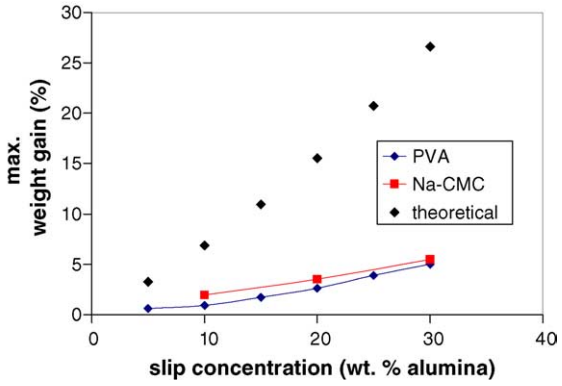

Fig. 15. Plateau weight gain as a function of slip concentration and time of the sintered samples.

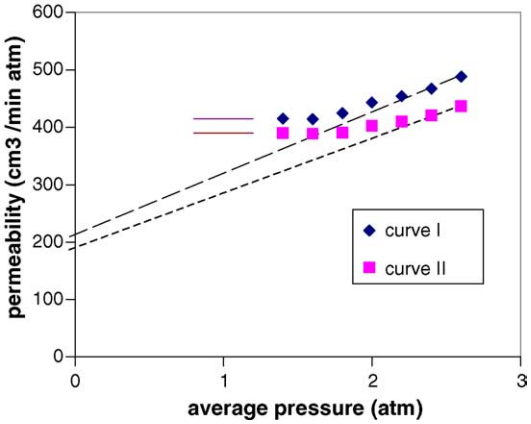

Fig. 16. Typical permeability curves for the substrate (I) and composite membrane (II) using a 10 wt.% slurry concentration, 12 s dip-coating time and Na-CMC as binder. The corresponding dashed lines (due to Knudsen regime) cross the vertical axis at $1/R_s^K$ and a, respectively. The slope of the corresponding solid lines (due to the Poiseuille regime) are $1/R_l^P$ and b, respectively.

pure Knudsen and pure Poiseuille flows are identified and individually used for the evaluation of the average permeable pore size and tortuosity ratio. In the present work, the same methodology is used but for the support-membrane composite structure. For the discussion that follows, refer to the typical permeability versus average pressure curves of the substrate (curve I, before dip coating) and composite membrane (curve II, after dip coating and sintering) shown in Fig. 16 (Na-CMC as binder, 10 wt.% slip concentration and 12 s dip-coating time). All the curves exhibit a Knudsen and Poiseuille flow region and this had been indicated.

The key point behind is that considering the Knudsen flow regime of the composite membrane, it is certain that both the flow in the substrate and in the membrane layer are of the Knudsen type. The same is true for the Poiseuille flow regime. It should be emphasized that previous works dealing with the characterization of micro, nano and ultrafilters through the gas permeation method used the "transition flow regime", where both Knudsen and Poiseuille flow play a role and permeability changes linearly with the average pressure.[11,12] According to Fig. 16, the slope of the transition zone between Knudsen and Poiseuille regime is not constant (nonlinear relationship), and therefore, a more robust method is needed.

Considering first the Knudsen regime of curve I, the permeability of the substrate may be evaluated as:

$$\frac{Q P_0}{A(P_1 - P_2)} = \frac{1}{R_s^K} \tag{3}$$

where Q is the flow rate($m^3\,s^{-1}$); P_0, the atmospheric pressure (Pa); A, the membrane area (m^2); P_1, the inlet pressure (Pa); P_2, the pressure at the substrate–membrane layer interface (Pa); and R_s^K, the Knudsen flow resistance of the substrate ($s\,m^{-1}$). The value of $1/R_s^K$ can be evaluated from the experimental curve due to the substrate only (curve I, dashed line).

The permeability of the membrane layer is:

$$\frac{Q P_0}{A(P_2 - P_3)} = \frac{1}{R_l^K} \tag{4}$$

where P_3 is the composite membrane outlet pressure (Pa) and R_l^K is the Knudsen flow resistance of the membrane layer ($s\,m^{-1}$). R_l^K is unknown. On the other hand, considering the horizontal section of the permeability curve belonging to the composite layer, we get:

$$\frac{Q P_0}{A(P_1 - P_3)} = a \tag{5}$$

where a is a known experimental constant. Combining Eqs. (3)–(5), we obtain:

$$\frac{1}{R_l^K} = \frac{a}{1 - aR_s^K} \tag{6}$$

Considering the Poiseuille flow region, the permeability of the substrate is:

$$\frac{Q P_0}{A(P_1 - P_2)} = \frac{1}{R_s^P}\frac{1}{2}(P_1 + P_2) \tag{7}$$

where R_s^P is the Poiseuille flow resistance of the substrate ($Pa\,s\,m^{-1}$). The value of $1/R_s^P$ can be evaluated from the experimental curve due to the substrate only (curve I, solid line). The permeability of the membrane layer is:

$$\frac{Q P_0}{A(P_2 - P_3)} = \frac{1}{R_l^P}\frac{1}{2}(P_2 + P_3) \tag{8}$$

where R_l^P is the Poiseuille flow resistance of the membrane layer ($Pa\,s\,m^{-1}$). R_l^P is unknown. Then, considering the Poiseuille flow regime of curve II for the composite layer, we get:

$$\frac{Q P_0}{A(P_1 - P_3)} = b\frac{1}{2}(P_1 + P_3) \tag{9}$$

where b is a known constant. Then, combining Eqs. (7)–(9), the following relation may be obtained:

$$\frac{1}{R_l^P} = \frac{b}{1 - bR_s^P} \tag{10}$$

The membrane-layer effective pore radius is then evaluated as below:

$$r = \frac{16\eta[8RT/\pi M]^{0.5} R_l^K}{3R_l^P} \tag{11}$$

where r is the effective pore radius (m); η, the gas viscosity ($kg\,m^{-1}\,s^{-1}$); R, the universal gas constant ($j\,mole^{-1}\,K^{-1}$); T, the temperature (K) and M, the gas molecular weight ($kg\,kgmole^{-1}$).

Using Eqs. (6), (10) and (11), pore effective diameters have been calculated for different series of membranes produced using PVA and Na-CMC as binder. The results for the effective pore diameter are shown in Table 2. Generally speaking, pore diameters are within the range of 0.08–0.14 μm. From the data presented in Table 2, no strong correlation between slip concentration and pore size for a specific binder can be deduced. This means that although the degree of layer microstructure inhomogeneity and size of maximum pores between samples may be different, but the effective pore size lies within a narrow region and is less affected. The effective pore diameter is dictated by the size of the smallest connected pores.[13] By definition, microfilters have an effective pore diameter in the range of 0.05–2 μm. Hence, the prepared membranes could be appropriate for bacteria microfiltration where the pore size should be smaller than 0.2 μm.

Table 2
Effective pore diameter calculated using Eqs. (5), (9)–(11) for the sintered membrane layers

Number	Binder compound	Dip-coating time (s)	Slip concentration (wt.%)	Effective pore diameter (μm)
1	PVA	2	20	0.14
2	PVA	4	20	0.11
3	PVA	12	20	0.10
4	PVA	4	10	0.08
5	PVA	4	30	0.10
6	Na-CMC	2	10	0.09
7	Na-CMC	4	10	0.10
8	Na-CMC	8	10	0.11
9	Na-CMC	2	20	0.11
10	Na-CMC	4	20	0.10
11	Na-CMC	8	20	0.13

4. Conclusions

Using PVA as binder and in a range of slip concentration between 5 and 30 wt.%, dip-coating takes place rather fast and saturation is achieved at times lower than 2 s. In these systems, slip concentration is the main controlling parameter of the wet membrane layer thickness. Instead, using Na-CMC as binder, it is possible to control the layer thickness for a constant slip concentration changing the dip-coating time. The effective pore diameter, within the experimental conditions studied, falls within a narrow size range of 0.08–0.14 μm and is not affected significantly by the slip concentration, dip-coating time or kind of binder.

The open porosity of the membrane layers is a function of slip concentration and increases with slip concentration increase, independent of type of binder. The final roughness is at least 2.5 times larger than that of the substrate (both for PVA and Na-CMC). Hence, if used as intermediate layers, a polishing step might be essential.

A new method for the characterization of the membrane layer based on gas permeation has been presented and the pertaining equations derived. The method is applicable if permeability measurements embrace both Knudsen and Poiseuille flow regimes.

References

1. Fundamentals of inorganic membrane science and technology. In *Membrane Science and Technology Series 4*, ed. A. J. Burggraaf and L. Cot. Elsevier, 1996 [Chapter 6].
2. Morgart, J., Filson, J. L., Peters, J. J. and Bhave, R. R., US Patent 5242595, 1993.
3. Gu, Y. and Meng, G., A model for ceramic membrane formation by dip-coating. *J. Eur. Ceram. Soc.*, 1999, **10**, 1961–1966.
4. Falamaki, C., Naimi, M. and Aghaie, A., Dual behaviour of $CaCO_3$ as a porosifier and sintering aid in the manufacture of membrane/catalyst supports. *J. Eur. Ceram. Soc.*, 2004, **24**, 3195–3201.
5. Falamaki, C., Aghaie, A. and Ardestani, N. R., RBAO membranes/catalyst supports with enhanced permeability. *J. Eur. Ceram. Soc.*, 2001, **21**, 2267–2274.
6. Hsieh, H. P., Inorganic membranes for separation and reaction, *Membrane Science and Technology Series 3*. Elsevier, 1996 [Chapter 4].
7. Tiller, F. M. and Tsai, C. D., Theory of filtration of ceramics. I. Slip casting. *J. Am. Ceram. Soc.*, 1986, **69**(12), 882–887.
8. Zheng, J. and Reed, J. S., Effects of particle packing characteristics on solid-state sintering. *J. Am. Ceram. Soc.*, 1989, **72**(5), 810–817.
9. Lindquist, K. and Liden, E., Preparation of alumina membrane by tape casting and dip coating. *J. Eur. Ceram. Soc.*, 1997, **17**, 359–366.
10. Falamaki, C., Shafiee Afarani, M. and Aghaie, A., Initial sintering stage pore growth mechanism applied to the manufacture of ceramic membrane supports. *J. Eur. Ceram. Soc.*, 2004, **24**, 2285–2292.
11. Lin, Y. S. and Burggraaf, A. J., Preparation and characterization of high temperature thermally stable alumina composite membrane. *J. Am. Ceram. Soc.*, 1991, **74**(1), 219–224.
12. Uchityl, P., Gas separation in ceramic membranes. Part I. Theory and testing of ceramic membranes. *J. Membr. Sci.*, 1994, **97**, 139–144.
13. Falamaki, C., Agahie, A. and Ardestani, N. R., RBAO membranes/catalysts supports with enhanced permeability. *J. Eur. Ceram. Soc.*, 2001, **21**, 2267–2274.